



Non-thermal effects on H- α emission in the flare 25 July 2004

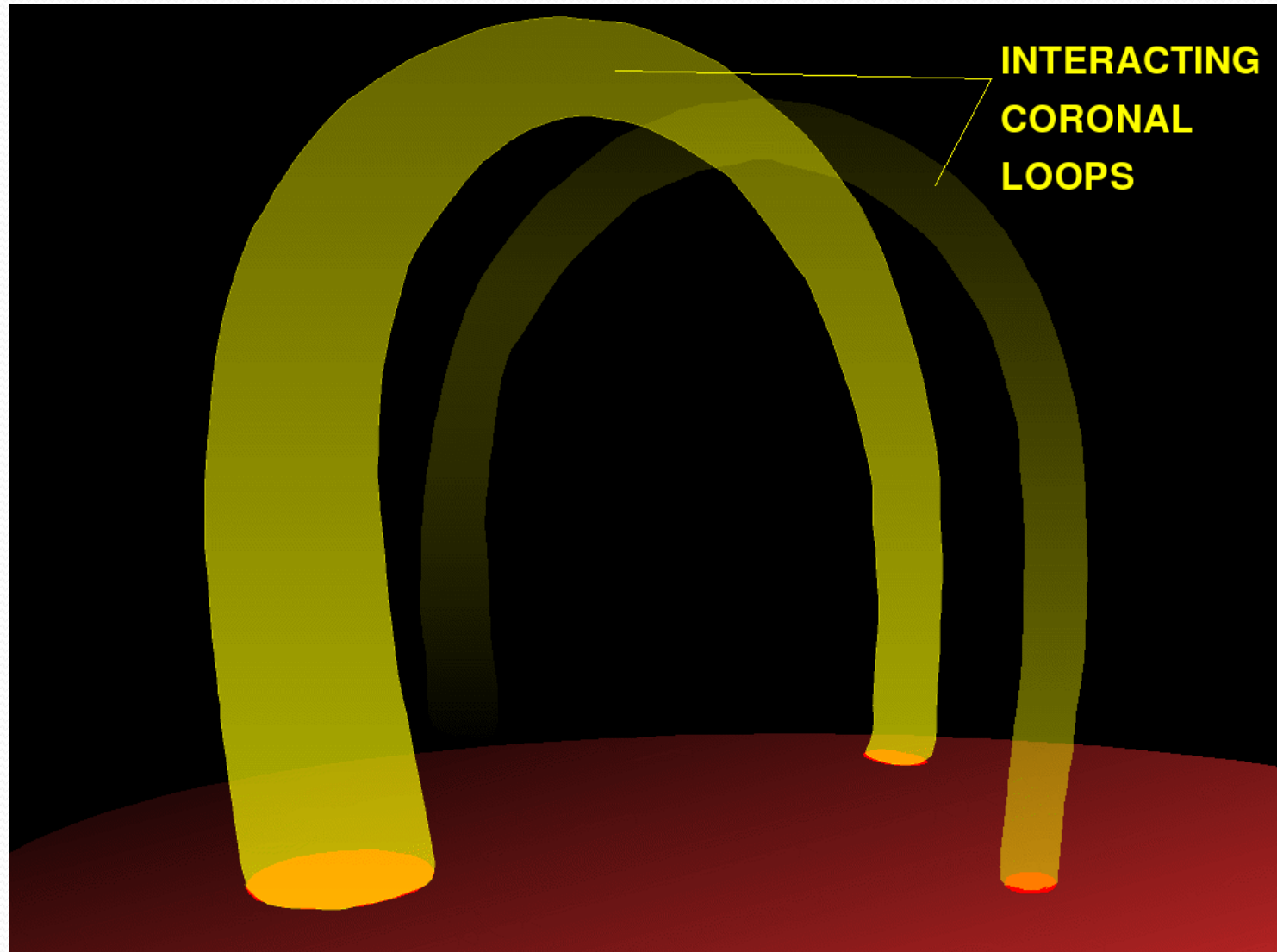
Zharkova V.V. (1), Kashapova L.K.(2), Chornogor S. (3),
Andrienko O. (3)

1 – Dept. of Mathematics, University of Bradford, UK

2 – Dept. of Radio-physics, ISTP, Irkutsk, Russia

3 – Solar Physics Dept., MAO, Kiev, Ukraine

Solar flare mechanisms



Non-thermal H ionisation & excitation and its effect on Ni

- By beam electrons (Hudson, 1972, Aboudraham & Henoux, 1986,87; Zharkova & Kobylinsky, 1989,91,Sol.Phys,93; Zharkova et a;., 2007)
- By beam protons (Henoux et al, 1993, Voigt et al., 1996)
- Full non-LTE radiative transfer for 5 level plus continuum Hydrogen atom
- Predicted increase in Hydrogen lines and especially in Paschen continuum
- Recent review by Fletcher et al (2010) – much more attention was paid to non-thermal effects

Non-thermal hydrogen excitation/ionisation rates

HYDROGEN EMISSION IN IMPULSIVE SOLAR FLARES

265

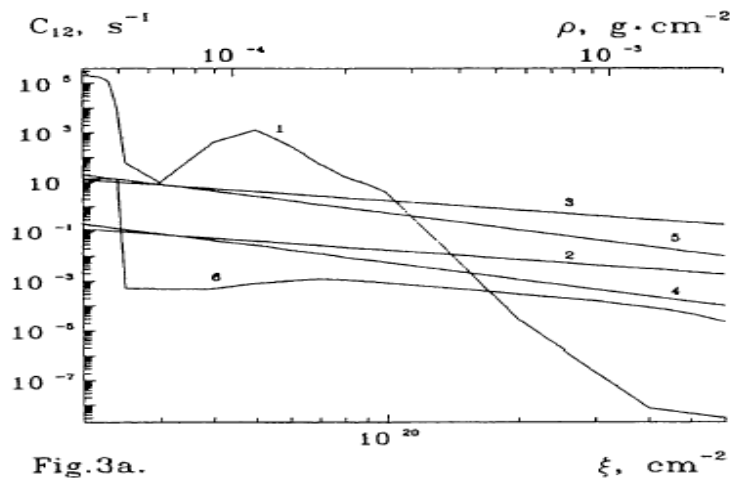


Fig.3a.

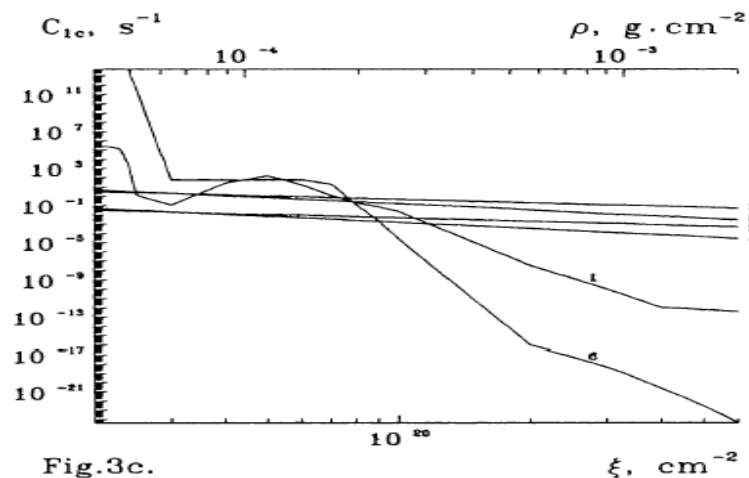


Fig.3c.

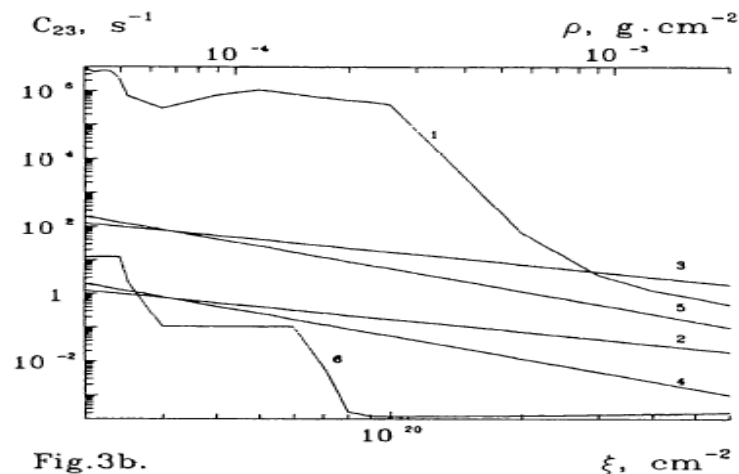


Fig.3b.

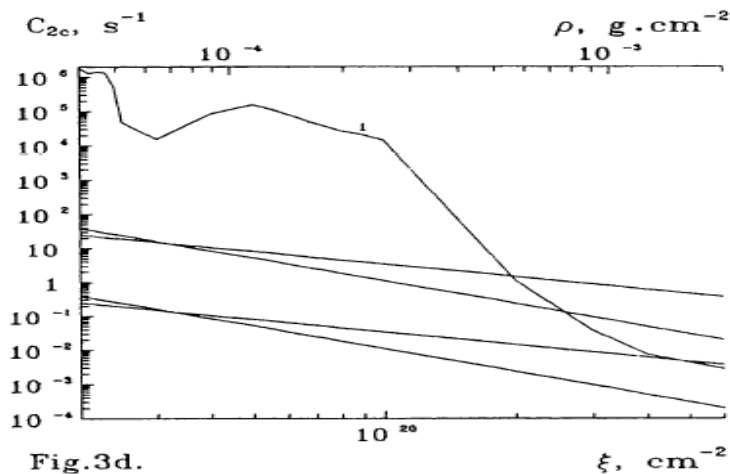


Fig.3d.

Fig. 3. A comparison of the elementary process rate depth variations (radiative and collisional) in the impulsive event model for 2.5 s: (a) 1 → 2, (b) 2 → 3, (c) 1 → c (continuum), (d) 2 → c. The numbers in the curves denote the parameters: 1 - pure thermal; 2 - $\gamma = 3$, $F_0 = 10^9$ (erg cm⁻² s⁻¹); 3 - $\gamma = 3$, $F_0 = 10^{11}$; 4 - $\gamma = 5$, $F_0 = 10^9$; 5 - $\gamma = 5$, $F_0 = 10^{11}$; 6 - external radiation.

H excitation/ionisation rates by e-beam

(Zharkova and Kobylinskij, Solar Phys., 1993)

TABLE I. Comparison of Excitation and Ionization Rates ($B_{nn'}$, B_{nc}) of a Hydrogen Atom for Beam Electrons with $\gamma = 3$ (first row) with Analogous Rates for "Thermal" Electrons

n	n'=2	3	4	5	6	c
1	0.162-07 * 0.206-12 0.941-16	0.389-08 0.611-14 0.634-18	0.138-08 0.108-14 0.682-19	0.655-09 0.371-15 0.185-19	0.364-09 0.173-15 0.785-20	0.615-08 0.709-15 0.150-19
2		0.326-06 0.635-07 0.131-07	0.714-07 0.646-08 0.927-09	0.262-07 0.170-08 0.200-09	0.128-07 0.702-09 0.740-10	0.484-07 0.166-08 0.764-10
3			0.189-05 0.117-05 0.594-06	0.413-06 0.157-06 0.641-07	0.149-06 0.724-07 0.290-07	0.164-06 0.609-07 0.125-07
4				0.636-05 0.541-05 0.341-05	0.146-05 0.819-06 0.471-06	0.393-06 0.335-06 0.120-06
5					0.159-04 0.774-06 0.950-06 0.449-06	0.774-06 0.950-06 0.449-06

*Read as $0.162 \cdot 10^{-7}$.

$$C_{nn'} = N_e B_{nn'} \text{ sec}^{-1}, \quad (1)$$

$$B_{nn'} = \sqrt{\frac{2}{m}} \int_{E_0}^{\infty} \sqrt{E} f(E) \sigma_{nn'}(E) dE \text{ cm}^3/\text{sec}, \quad (2)$$

$$N(E, \xi) = K E^{1/2} (E^2 + 2a\xi)^{-1/2} \theta(\sqrt{E^2 + 2a\xi} - E_1) \theta(E_2 - \sqrt{E^2 + 2a\xi}), \quad (3)$$

$$N_e^F(\xi) \approx \frac{F_0 \left(\frac{m}{2}\right)^{1/2}}{(E_2^{2-\gamma} - E_1^{2-\gamma})} \frac{2-\gamma}{2} (2a\xi)^{\frac{1-2\gamma}{4}} \frac{\Gamma\left(\frac{3}{4}\right) \Gamma\left(\frac{2\gamma-1}{4}\right)}{\Gamma\left(\frac{\gamma+1}{2}\right)}, \quad (4)$$

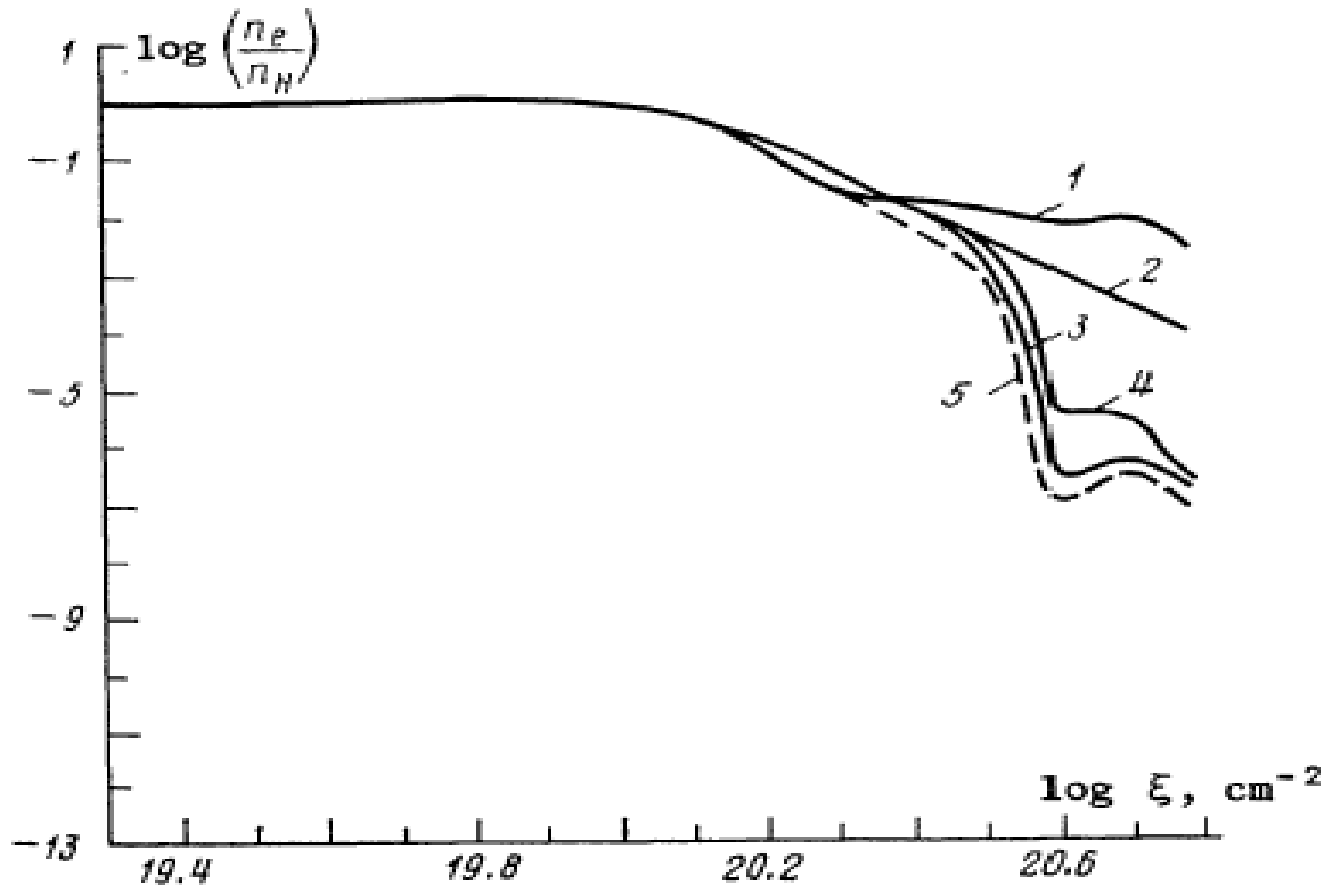


FIG. 3. Depth (ξ) distribution of the degree of ionization of hydrogen atoms for the same values of initial energy flux F_0 at the boundary ($\text{ergs} \cdot \text{cm}^{-2} \cdot \text{sec}^{-1}$) and spectral indices γ : 3) $\gamma = 5$, $F_0 = 10^9$; 4) $\gamma = 5$; $F_0 = 10^{12}$; 1, 2, 5) see caption of Fig. 1.

Lyman line profiles affected by non-thermal excitation

268

V. V. ZHARKOVA AND V. A. KOBYLINSKY

We take into account radiative and collisional (thermal and non-thermal) processes. The absorption coefficient profiles are suggested to be the Voigt ones in the lines, and to be equal to $f(\nu) = \nu_c^3/\nu^3$ in the Ly- and Ba-continua, where ν_c is the continuum head frequency. The spontaneous recombination rates were taken according to Burgess (1964).

In Figures 3 and 4 and in Figures 5–8 there are presented the hydrogen $L\alpha$, $L\beta$, and $H\alpha$ lines intensities and the intensity distributions and inclination in the heads of the Ly, Ba, and Pa-continua respectively for the accepted physical models through 1 s, 2.5 s, and 4 s after beginning of electron beam injection.

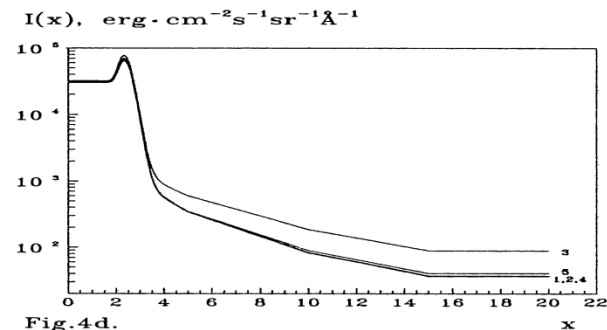
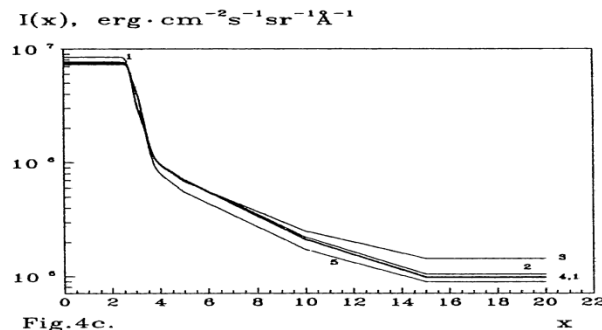
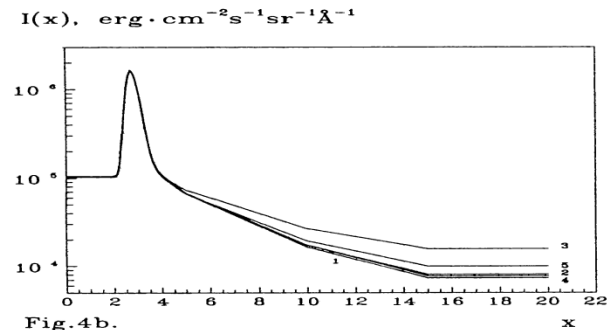
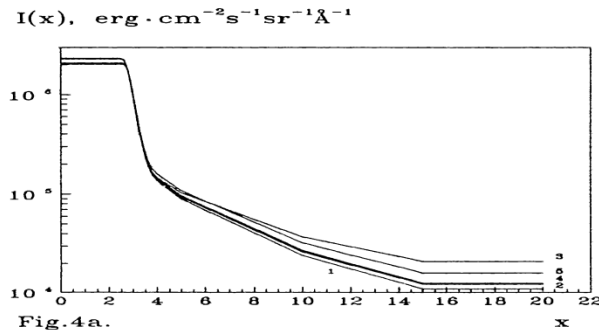


Fig. 4. The $L\alpha$ and $L\beta$ line intensities computed for different flare models: (a) time 1 s ($L\alpha$ line), (b) time 2.5 s ($L\alpha$), (c) 4 s ($L\alpha$), (d) 2.5 s ($L\beta$). Here and thereafter up to Figure 8 the numbers at the curves are the same as in Figure 3.

Balmer line profiles affected by non-thermal excitation

HYDROGEN EMISSION IN IMPULSIVE SOLAR FLARES

269

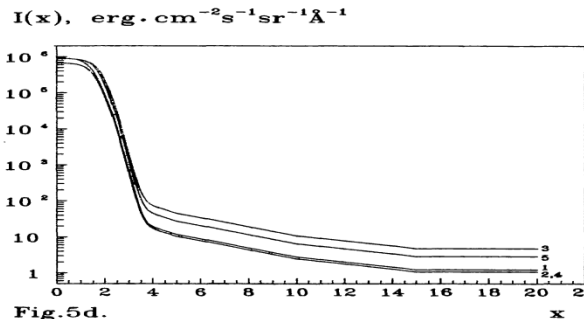
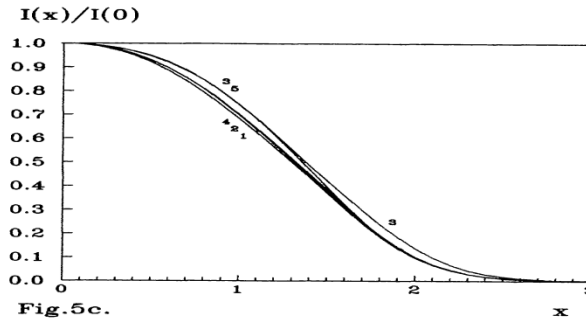
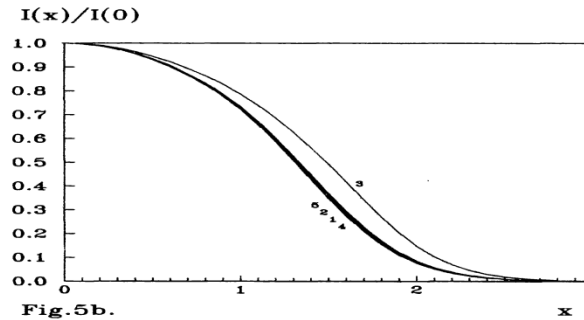
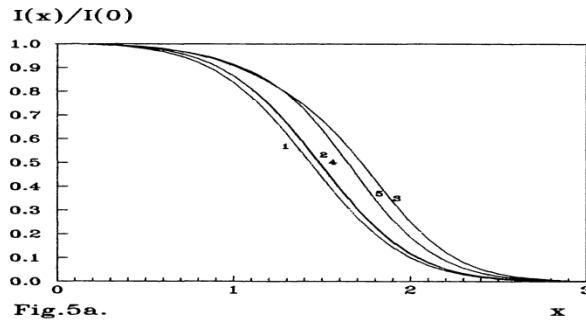


Fig. 5. The H α line intensities computed for the flare models with (a) $t = 1$ s (line cores), (b) $t = 2.5$ s (line cores), (c) $t = 4$ s (line cores), (d) $t = 1$ s (line wings).

At the first seconds of injection the effect of non-thermal impacts is pronounced in the high chromosphere. One sees that after the development of a gasdynamical response in the chromosphere (over 4 s), the influence of beam electrons on the line profiles, continuum intensity distributions, and inclinations is very sensitive to the relation between physical conditions and the beam parameters.

The hydrogen L α and L β line profiles are varying rather similarly to the flare gasdynamics. At the first second the line core intensities decrease for the low F_0 (10^9) and increase for the higher F_0 (10^{11}), in comparison with the pure thermal model. On the contrary, the wing intensities strongly depend on a spectral index γ , and less on the initial flux F_0 , arising with a decrease in γ and with an increase in F_0 .

Balmer continuum affected by non-thermal ionization

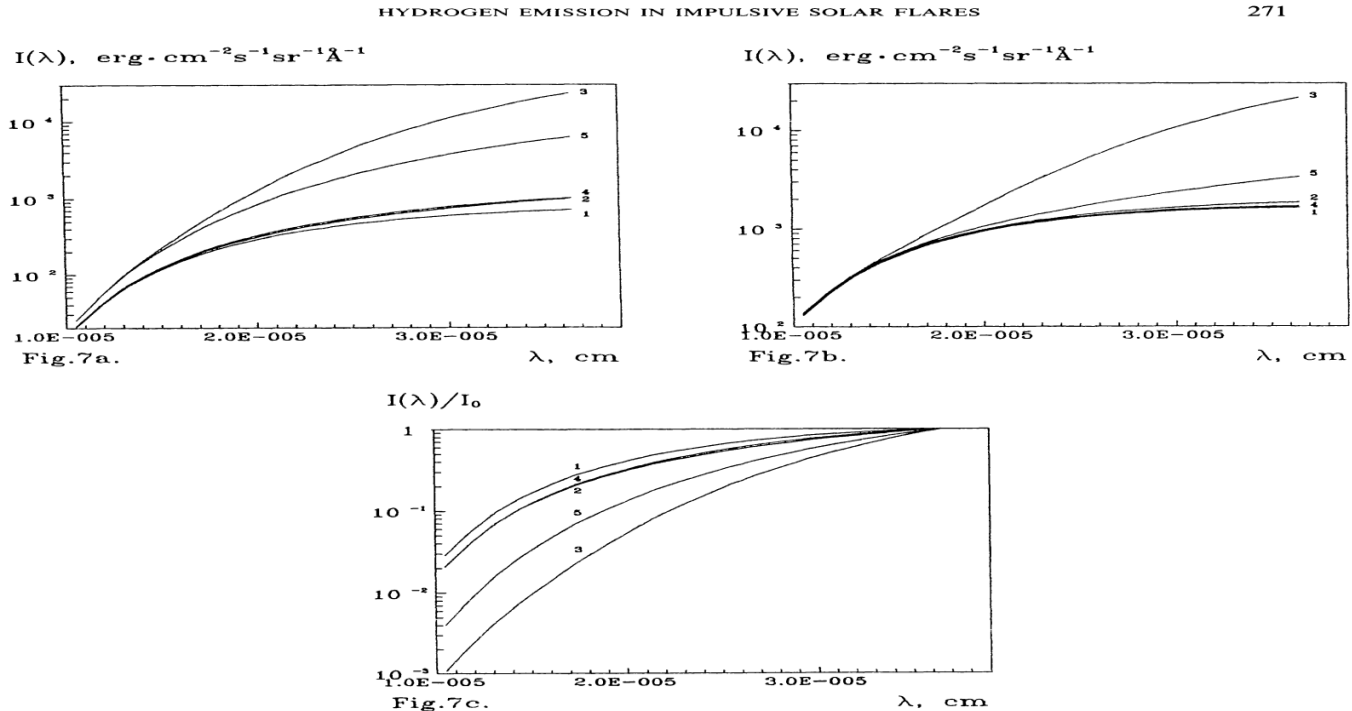


Fig. 7. The same as in Figure 6 for the Balmer continuum.

In general, it is possible to conclude that the effect of a beam of electrons on the hydrogen lines is mainly in the wings and for a detection of that, rather precise observations are needed.

The hydrogen continuum intensities are more sensitive to non-thermal impacts, as one can see from Figures 6–8. In spite of greater non-thermal ionization rates for the Ly-continuum, the intensity distributions (Figure 6) for a set of different beam parameters are rather close. A slight growth of the Ly-head intensity is observed with F_0 increasing and γ decreasing for any time, and the spectrum inclination is shown to decrease (see Figure 6(c)). The maximum variations are observed in the first second, then they merely decrease. It is explained by a possible growth of Ly-continuum head opacity which overlaps all the non-thermal and thermal impacts.

Pashen continuum affected by non-thermal ionization

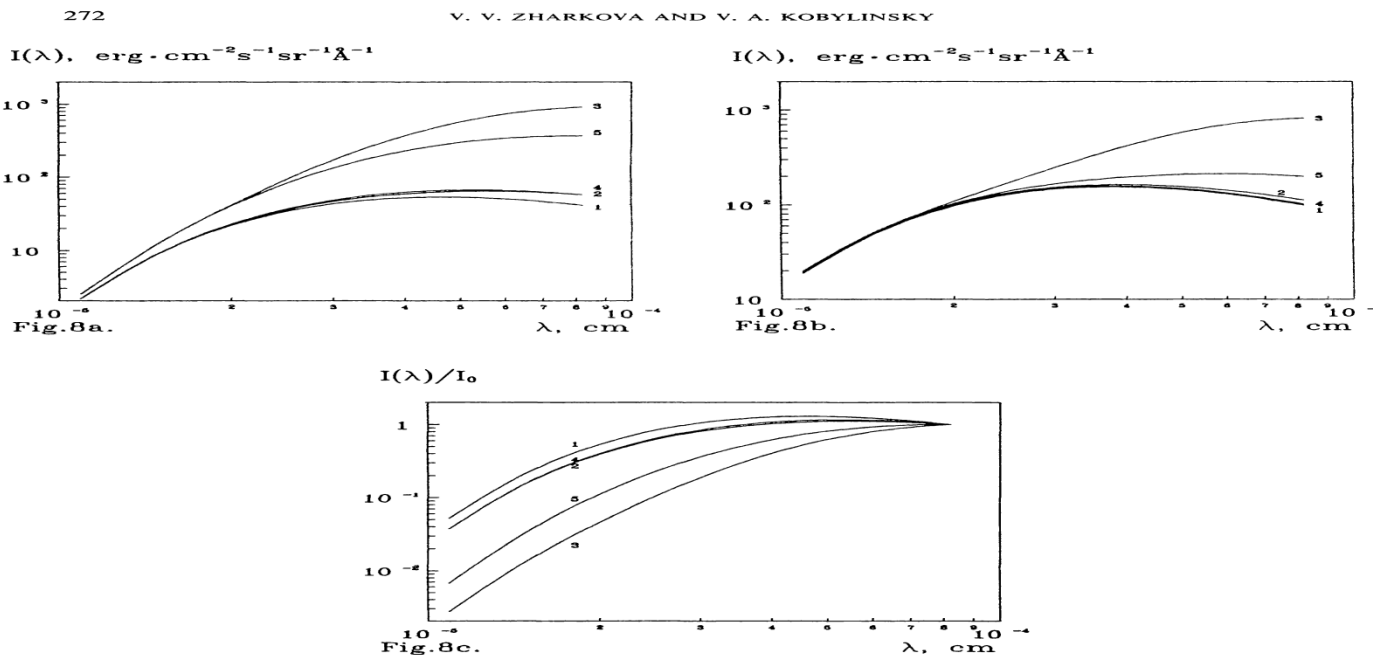


Fig. 8. The same for the Paschen continuum.

The Ba and Pa continuum intensity distributions (Figures 7 and 8) are strongly affected by non-thermal impacts. In the first second they engender the Ba and Pa-head intensities strong rising with F_0 growing and γ falling off. And the dependence of F_0 is more pronounced than of δ . Moreover, the head intensity inclinations are increased by the non-thermal impacts with beam electrons, and for beams with the initial fluxes F_0 equal to 10^{11} erg cm $^{-2}$ s $^{-1}$ and $\gamma = 3$ ($\delta = 4$) we can see almost a direct line in spite of the varying inclination over wavelength for other parameters. At other times (2.5 s and 4 s) the effect on Ba-continuum intensities is similar but smaller due to an increase of the thermal processes role via the gasdynamical response development. In a forthcoming paper we consider the joint effect of the hydrogen atoms and negative ions and

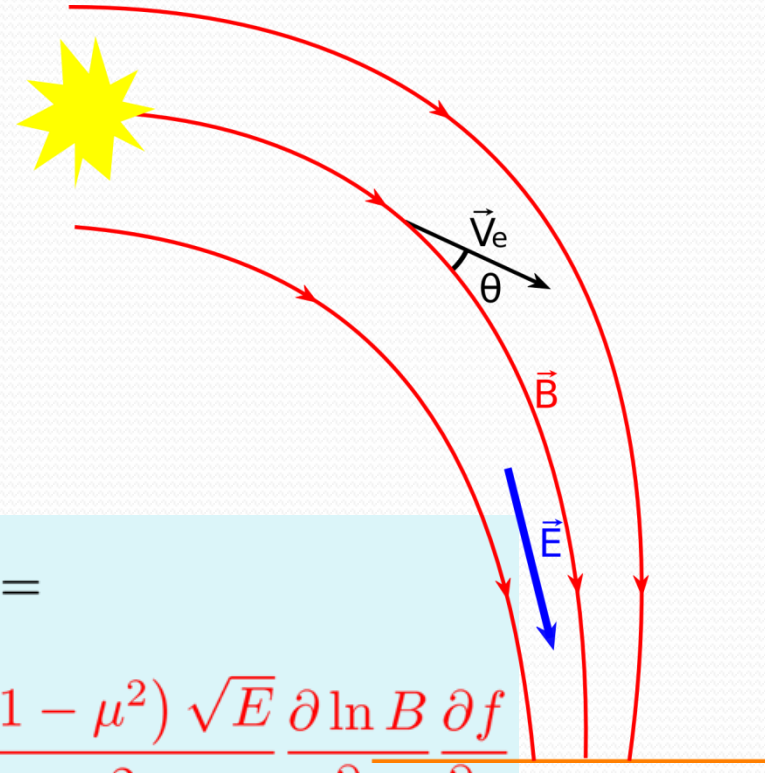
Fokker-Planck equation

$$f = f(t, s, E, \mu)$$

t – time

s – column depth

E – energy



self-induced (return current) electric field

$$\frac{\partial f}{\partial t} + n\sqrt{E}\mu \frac{\partial f}{\partial s} - 2\mathcal{E}\mu\sqrt{E} \frac{\partial f}{\partial E} - \mathcal{E} \frac{1-\mu^2}{\sqrt{E}} \frac{\partial f}{\partial \mu} =$$

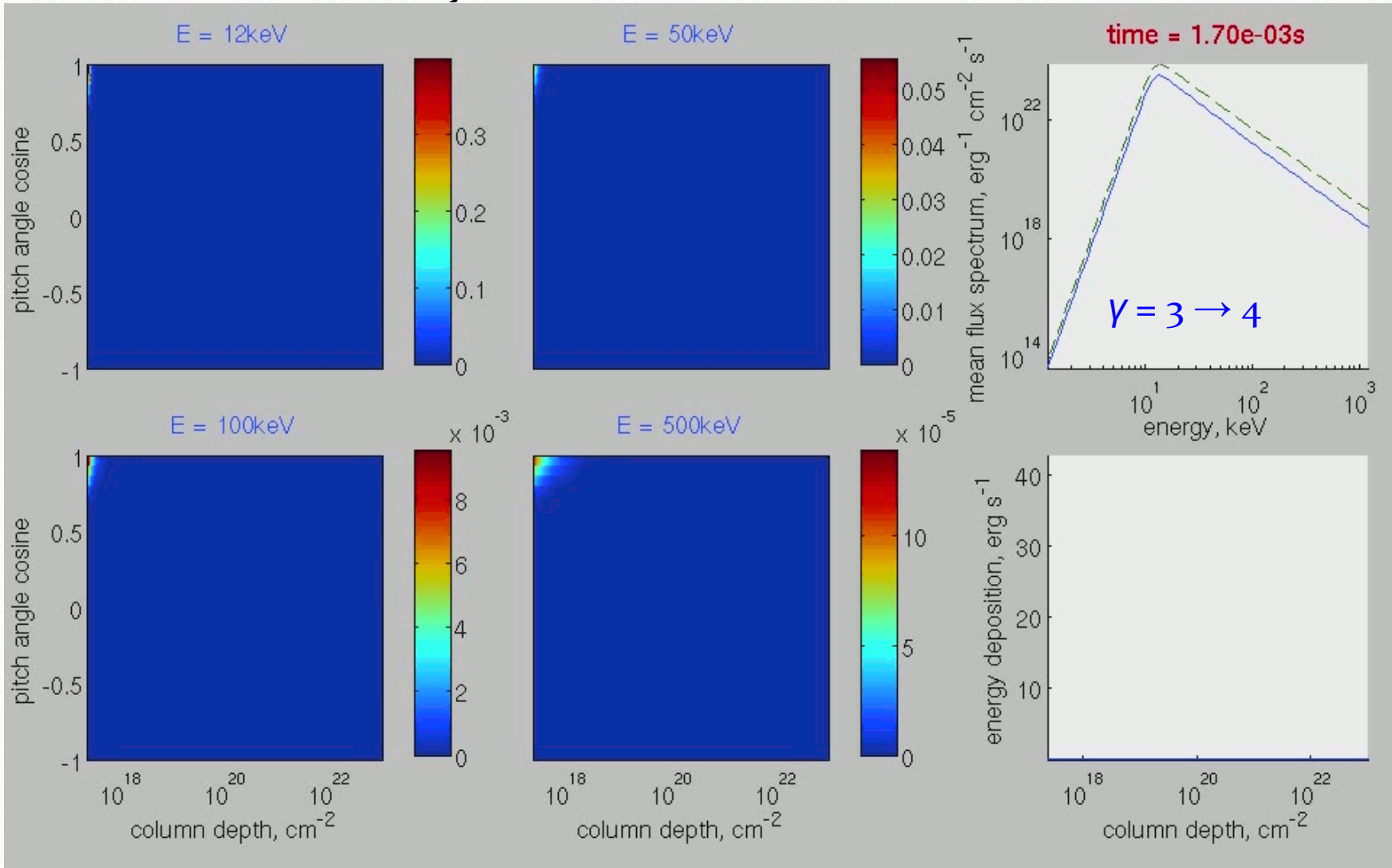
$$n \frac{1}{\sqrt{E}} \frac{\partial f}{\partial E} + n \frac{1}{2E^{3/2}} \frac{\partial}{\partial \mu} \left((1-\mu^2) \frac{\partial f}{\partial \mu} \right) - n \frac{(1-\mu^2)\sqrt{E}}{2} \frac{\partial \ln B}{\partial s} \frac{\partial f}{\partial \mu}$$

$$\mathcal{E} = \frac{j_{rc}(x)}{\sigma(x)} = \frac{j(x)}{\sigma(x)} = \frac{2\sqrt{2}\pi}{\sigma(x)} \frac{e}{\sqrt{m_e}} \int_0^\infty \int_{-1}^1 f(x, E, \theta) \sqrt{E} \cos \theta dE d \cos \theta$$

$n(s)$ and $T(s)$ are taken from the hydro-dynamic model (Zharkova, V. & Zharkov, S., ApJ, 664, 573, 2007)

Impulsive injection

$F_o = 10^{10} \text{ erg cm}^{-2} \text{ s}^{-1}$. Power law index is 3. Impulse length is $1.7 \cdot 10^{-3} \text{ s}$.
Only collisions are taken into account.



Stationary injection

Distribution function of the injected beam

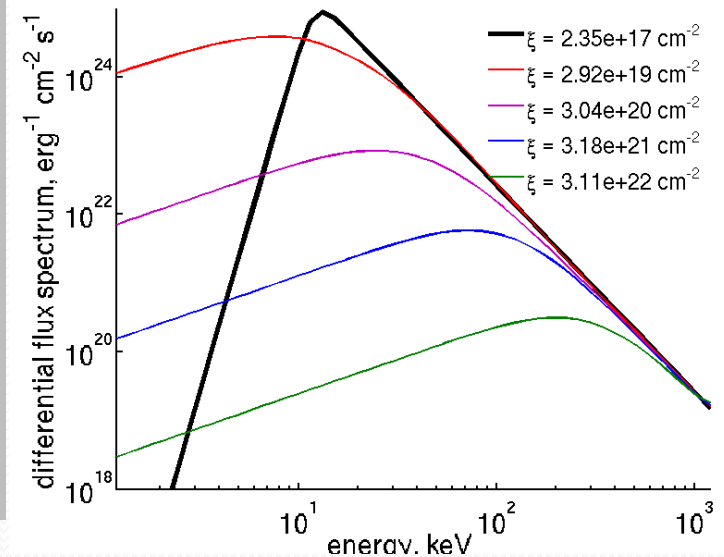
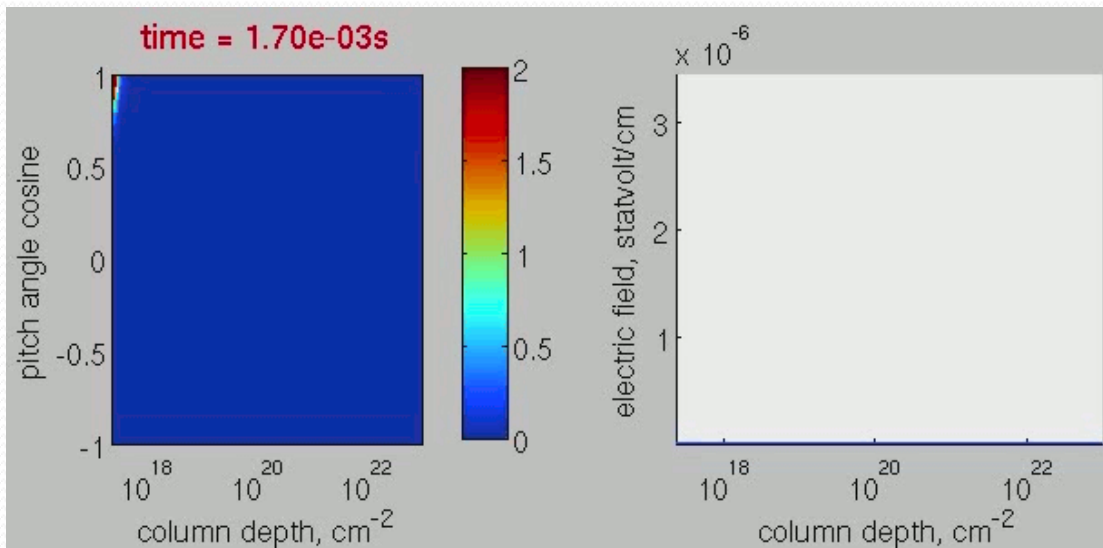
$$f(t, s = s_{min}, z, \mu > 0) = f_n \psi(t) \frac{E^{\delta-1}}{E^{\delta+\gamma} + E_0^{\delta+\gamma}} \exp\left(-\frac{(1-\mu)^2}{\Delta\mu^2}\right)$$

Initial power law index of high energy electrons $\gamma = 3$

Initial pitch angle dispersion $\Delta\mu = 0.2$

Lower energy cut-off $E_0 = 12$ keV

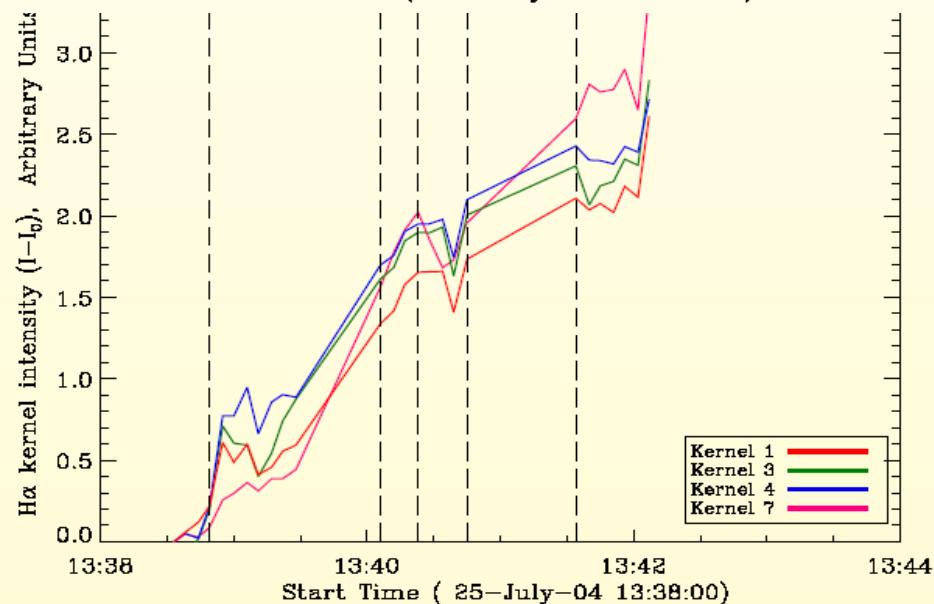
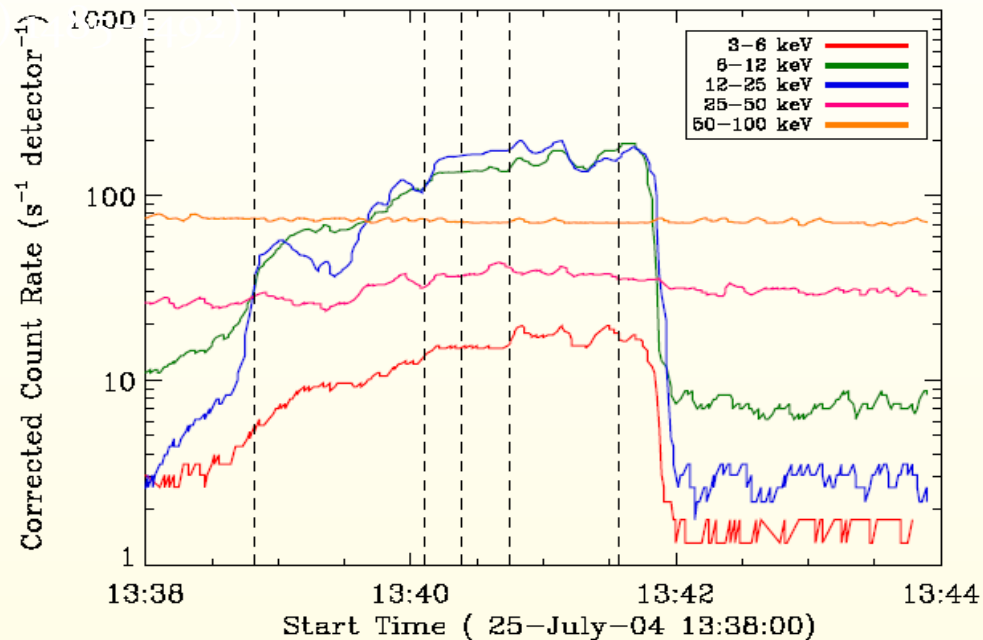
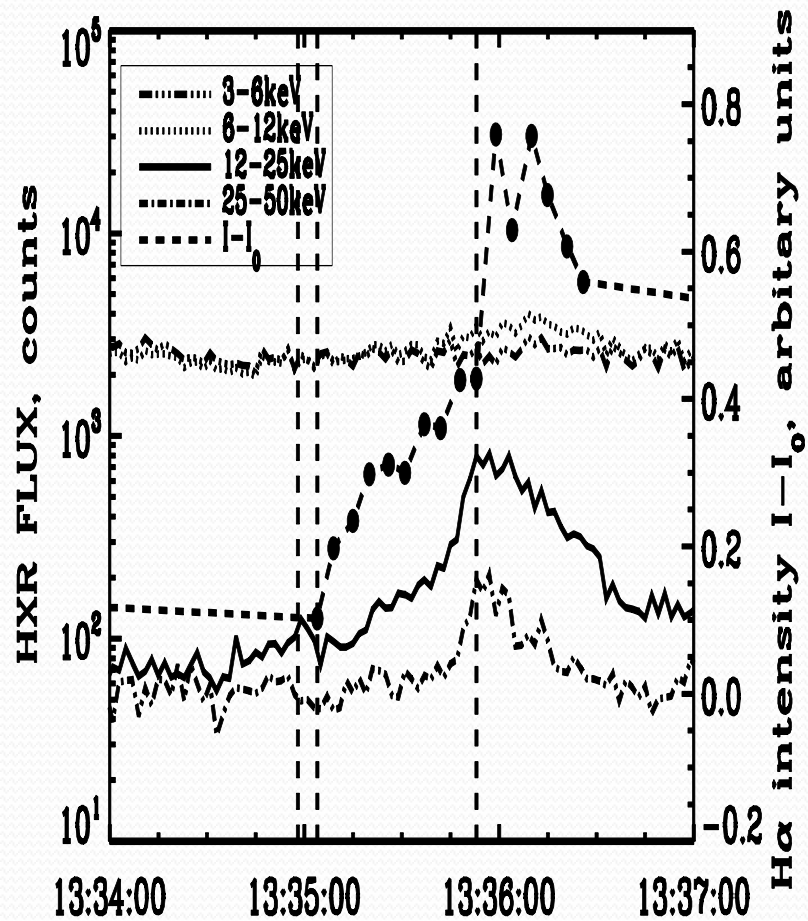
Energy flux on the top boundary is $F_0 = 10^{10}$ erg cm⁻² s⁻¹



Relaxation time is ≈ 0.07 - 0.1 s

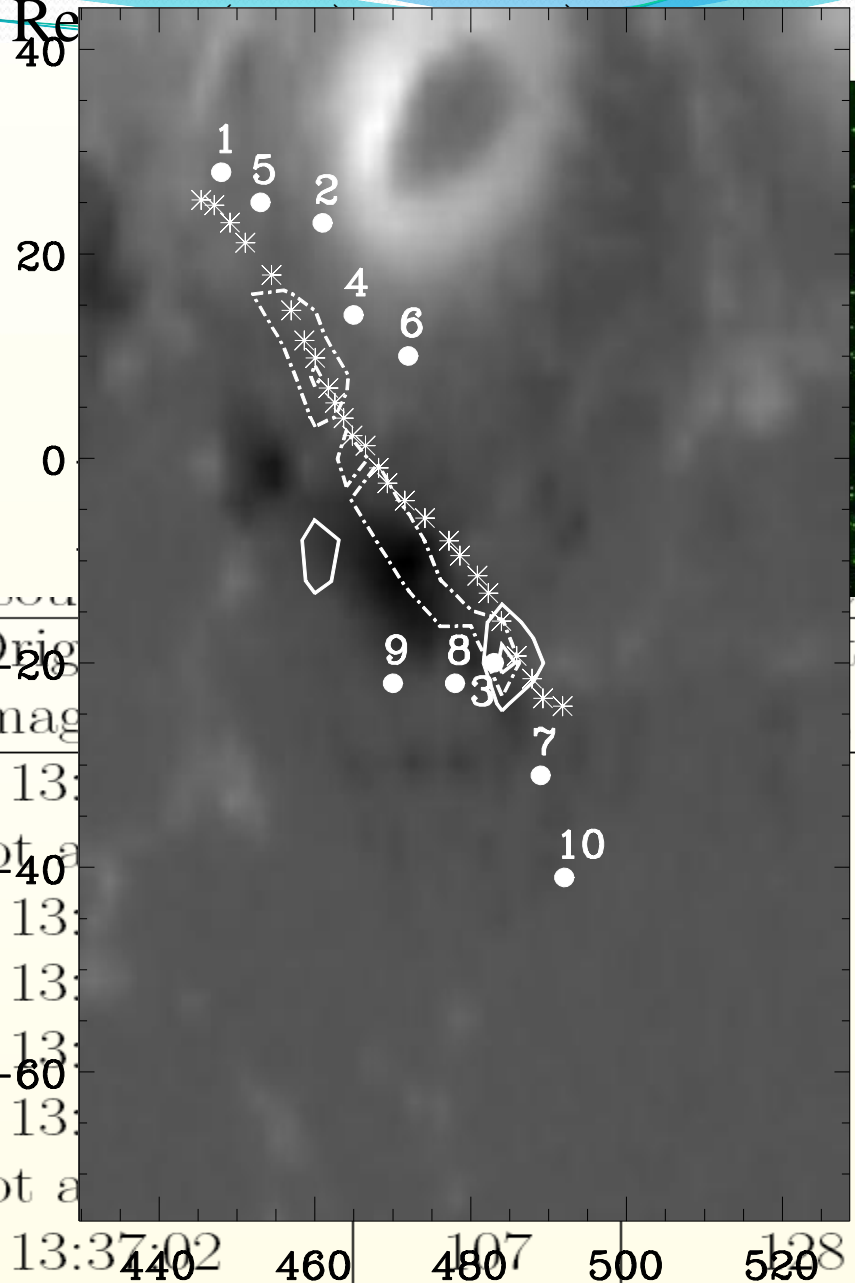
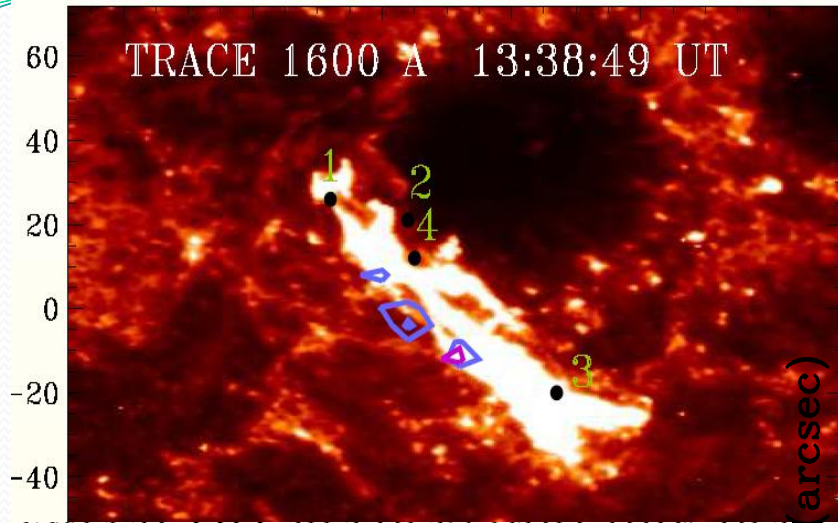
25 July 2004: The pre-flare (left) and main flare (right)

(Zharkova et al. MNRAS, 2010)



Images of the first phase of the flare

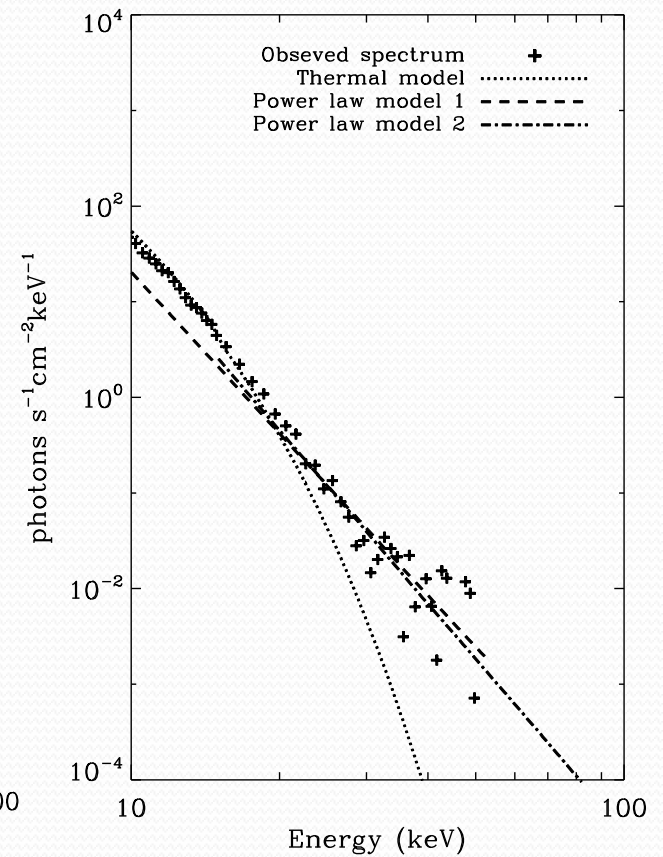
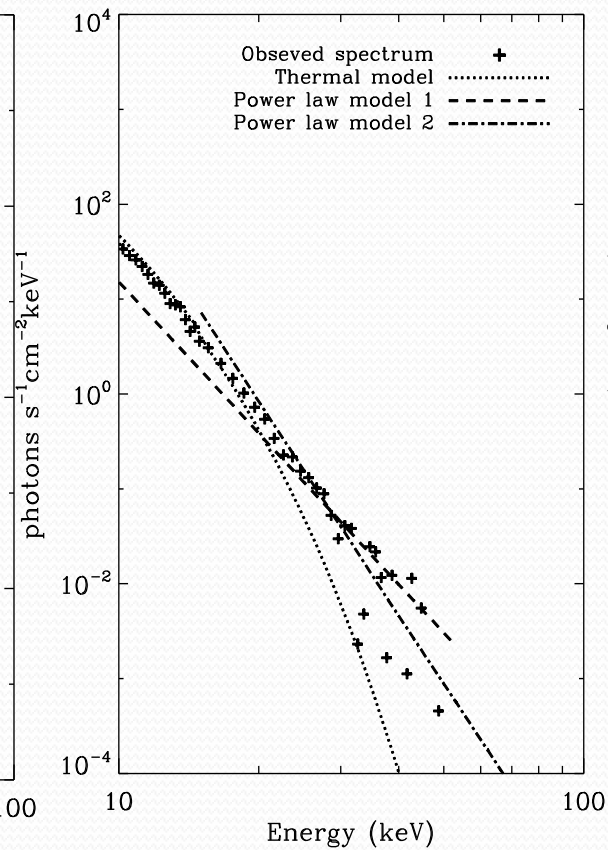
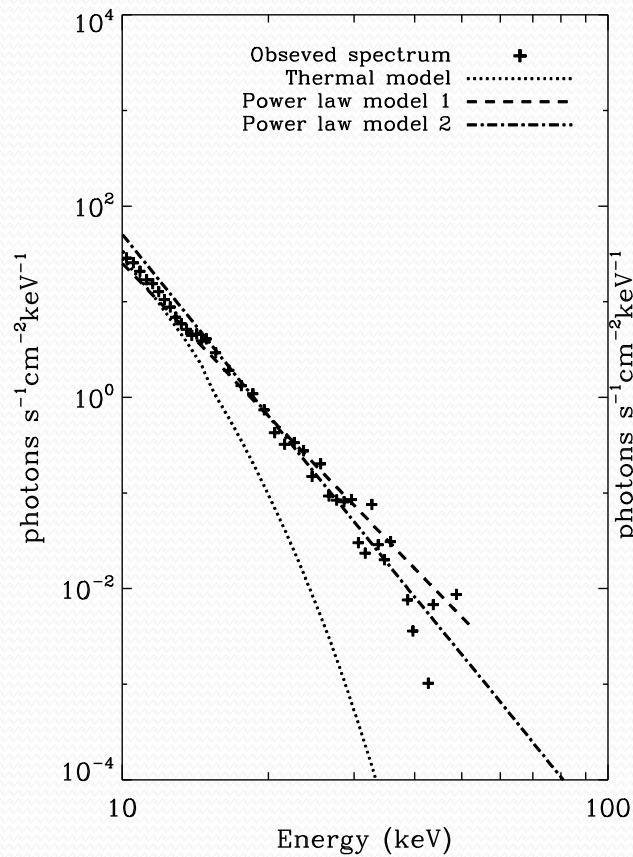
(Zharkova et al. AdvSpace Res



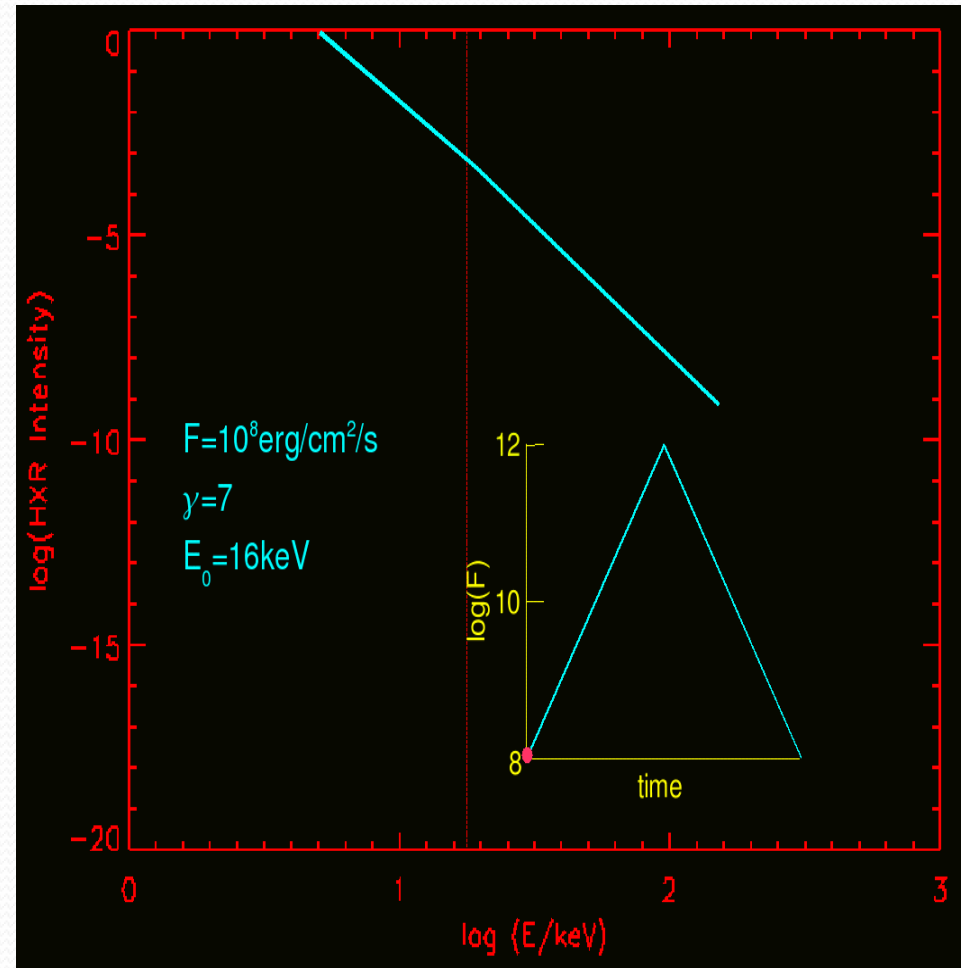
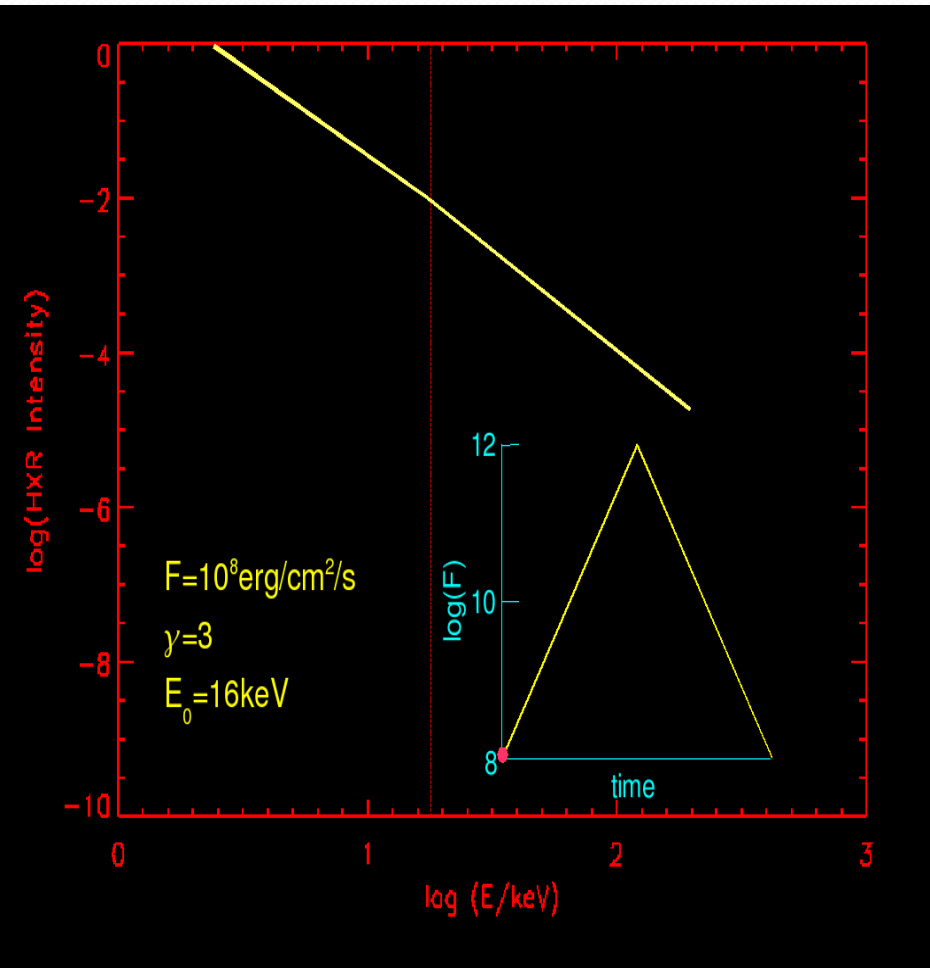
H α kernel	Time, UT	Polarity	Solar Y Origin
1	13:38:38	+	13:38:38
2	13:38:44	-	not a
3	13:38:49	-	13:38:49
4	13:38:55	+	13:38:55
5	13:40:06	+	13:40:06
6	13:40:06	+	13:40:06
7-9	>13:38:55	-	not a
10	13:41:40	-	13:41:40

HXR spectra for the 1st peak

Zharkova et al. MNRAS, 2010

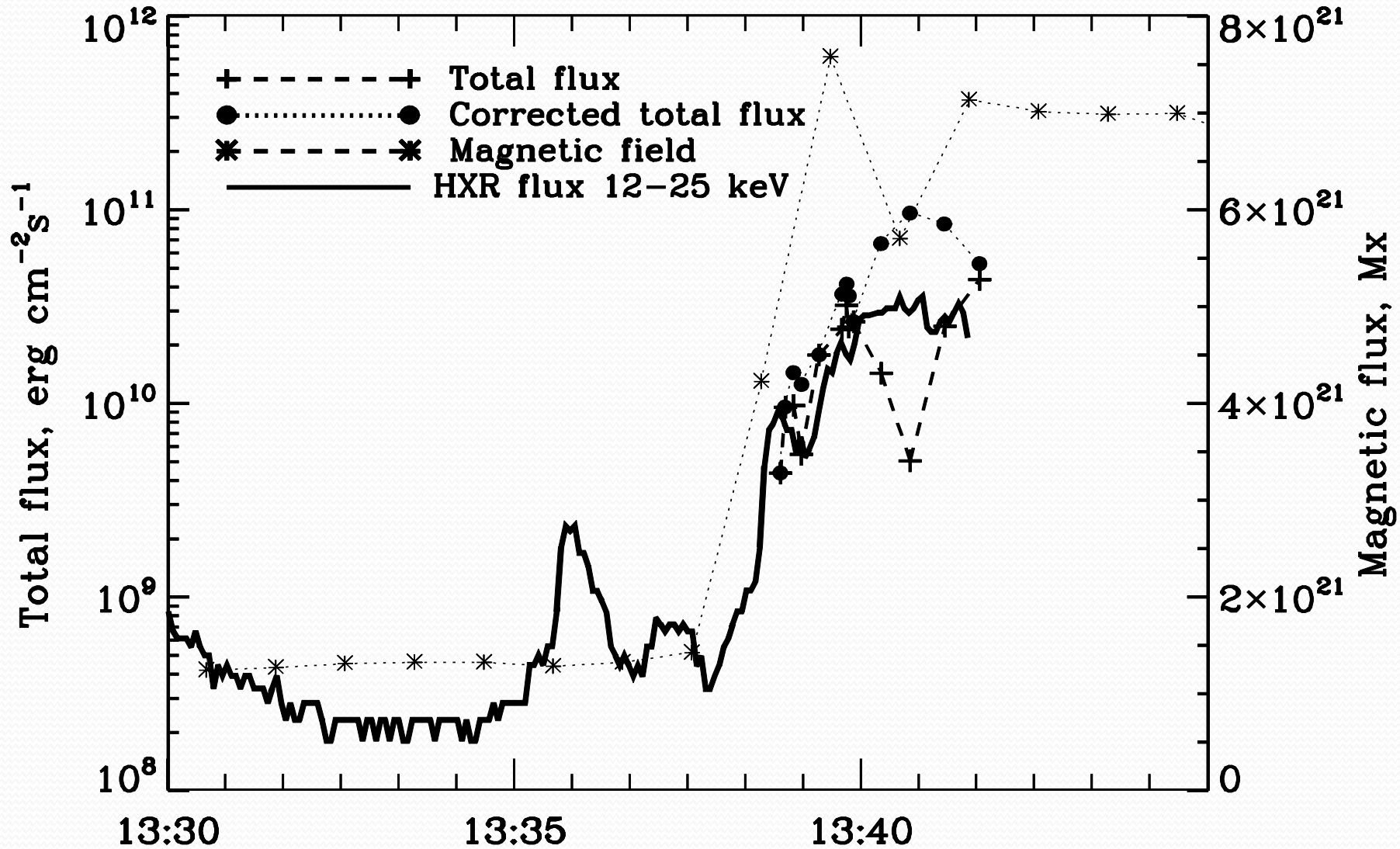


Photon energy spectrum as function electron beam parameters (RHESSEI nugget 25)



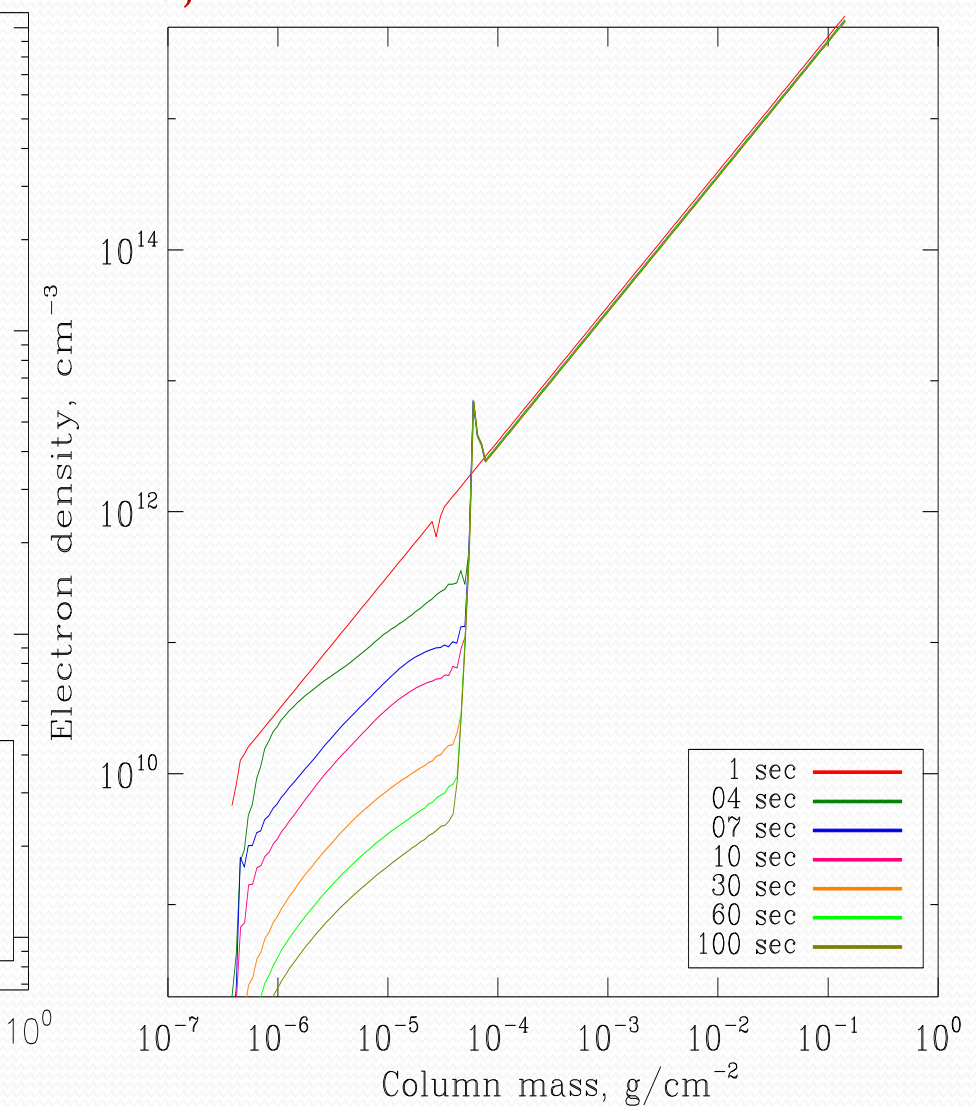
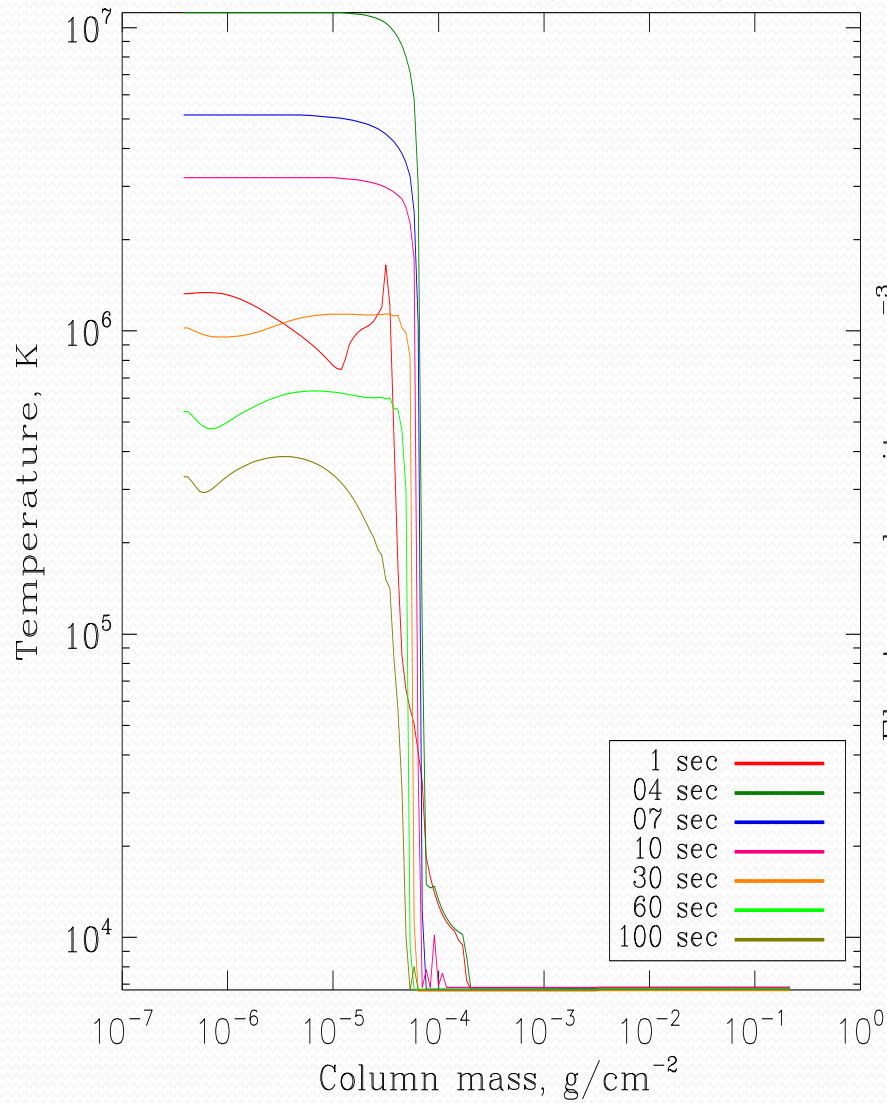
Correction of HXR photon flux for Ohmic losses –burst 1

Zharkova et al. MNRAS, 2010



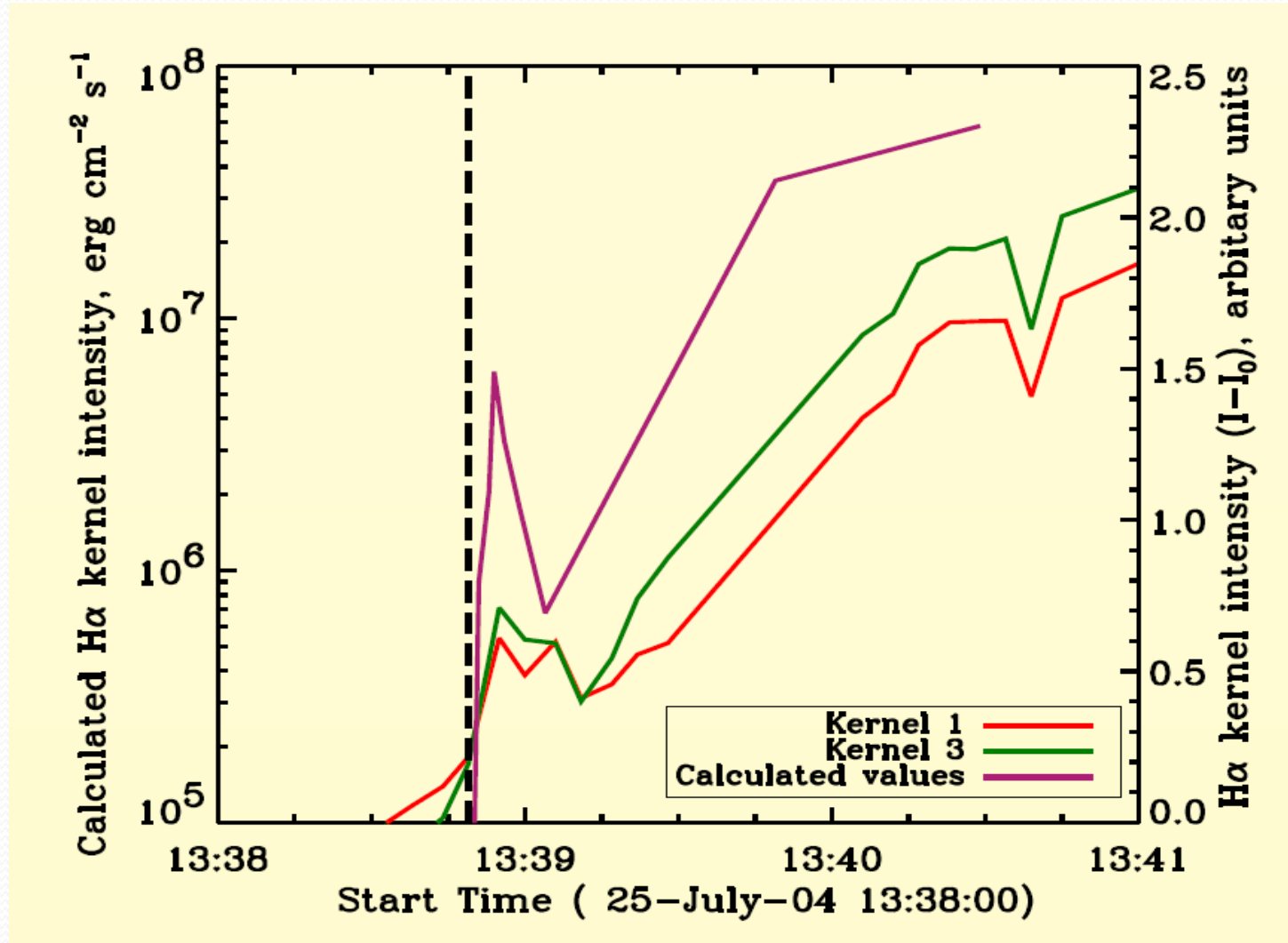
HD models for the burst one

Zharkova et al. MNRAS, 2010



H α line intensity (non-thermal + thermal excitation)

Kernels 1 и 3 (fit very well \rightarrow electrons are the agents)



Conclusions

- **Electron and proton beams naturally occur during a magnetic reconnection process**
- **Electrons and protons precipitate towards the chromosphere and photosphere**
- **High-energy particles have multiple effects on a flaring atmosphere:**
 - High energy emission (HXR, radio/MW)
 - Particles carry a charge → hence, electric field
 - Variations of electron electric field in space causes a transient magnetic field
 - Deposit energy into the ambient plasma via hydrodynamics
 - Produce non-thermal ionization and excitation → white light flares Paschen emission, Stark wings in Balmer emission, change Balmer increments, and many more appearing within seconds from HXR emission
 - As result electrons produce H-alpha emission increase prior any hydrodynamic heating